



Article

# An Open-Circuit Fault Diagnosis System Based on Neural Networks in the Inverter of Three-Phase Permanent Magnet Synchronous Motor (PMSM)

Kenny Sau Kang Chu , Kuew Wai Chew \*, Yoong Choon Chang and Stella Morris

Lee Kong Chian Faculty of Engineering and Science, Universiti Tunku Abdul Rahman, Jalan Sungai Long, Bandar Sungai Long, Kajang 43000, Malaysia; kc049507251@utar.my (K.S.K.C.); ycchang@utar.edu.my (Y.C.C.); stellam@utar.edu.my (S.M.)

\* Correspondence: chewkw@utar.edu.my

**Abstract:** Three-phase motors find extensive applications in various industries. Open-circuit faults are a common occurrence in inverters, and the open-circuit fault diagnosis system plays a crucial role in identifying and addressing these faults to enhance the safety of motor operations. Nevertheless, the current open-circuit fault diagnosis system faces challenges in precisely detecting specific faulty switches. The proposed work presents a neural network-based open-circuit fault diagnosis system for identifying faulty power switches in inverter-driven motor systems. The system leverages trained phase-to-phase voltage data from the motor to recognize the type and location of faults in each phase with high accuracy. Employing separate neural networks for each of the three phases in a three-phase permanent magnet synchronous motor, the system achieves an outstanding overall fault detection accuracy of approximately 99.8%, with CNN and CNN-LSTM architectures demonstrating superior performance. This work makes two key contributions: (1) implementing neural networks to significantly improve the accuracy of locating faulty switches in open-circuit fault scenarios, and (2) identifying the optimal neural network architecture for effective fault diagnosis within the proposed system.

**Keywords:** open-circuit fault (OCF); permanent magnet synchronous motor (PMSM); neural network



**Citation:** Chu, K.S.K.; Chew, K.W.; Chang, Y.C.; Morris, S. An Open-Circuit Fault Diagnosis System Based on Neural Networks in Inverter of Three-Phase Permanent Magnet Synchronous Motor (PMSM). *World Electr. Veh. J.* **2024**, *15*, 71. <https://doi.org/10.3390/wevj15020071>

Academic Editors: Jianguo Zhu, Yu Wang and Weiwei Geng

Received: 10 January 2024  
Revised: 8 February 2024  
Accepted: 12 February 2024  
Published: 16 February 2024



**Copyright:** © 2024 by the authors. Licensee MDPI, Basel, Switzerland. This article is an open access article distributed under the terms and conditions of the Creative Commons Attribution (CC BY) license (<https://creativecommons.org/licenses/by/4.0/>).

## 1. Introduction

Electric vehicles (EVs) have garnered significant attention due to their environmentally friendly characteristics and high efficiency [1]. The motor serves as the core source of energy, enabling the movement of the electric vehicle. Permanent magnet synchronous motors (PMSMs) have been popularly used in the electric vehicles industries [2]. Meanwhile, the inverter is responsible for controlling the motor's speed and direction. The failure of the inverter, which is caused by the failure of power switches, could reach approximately 30% [3,4]. It is important for the open-circuit fault diagnosis system (OCFDS) to check the system to ensure it is able to work under normal and safe conditions [5].

There are three main types of faults that can occur in motors: (1) mechanical faults, (2) electrical faults, and (3) magnetic faults [6–8]. This paper mainly focuses on electrical faults, which can arise from stator phase winding short circuits, open circuits, ground faults, and other issues. Short circuits in the winding are usually caused by wire insulation breakdown, overheating, or overload [9,10]. This paper's main focus is on open-circuit faults caused by driver problems, and proposed neural network-based open-circuit fault diagnosis system. Generally, the open-circuit fault diagnosis methods used for the inverter can be majorly classified into signal analysis processing methods, model-based methods, and data analysis methods [11,12]. Signal analysis processing methods use sensors to obtain the current or voltage in the phases for analysis [13]. By using the measured current and voltage to compute the fault detection index, the system can check for faults [14]. In [15],

current analysis was conducted to analyze fault and normal conditions. Subsequently, a conditioned table was created to represent the normal and faulty operation of the symmetrical components of the PMSM motor. The symmetrical components of the PMSM can be categorized into three types: (1) zero sequence, (2) positive sequence, and (3) negative sequence. To detect faults, the magnitude ratio of the positive sequence component to the negative sequence component was calculated to produce a fault detection index, which was utilized for fault type identification. Finally, the fault detection index was used in fault localization to determine the specific faulty switch. In [16], the open fault in the open winding motor fault diagnosis system was based on the differential-mode component to identify faults in the PMSM system. Through current analysis under faulty conditions, the zero sequence current and zero sequence voltage in the differential mode component were computed [16–18]. A zero sequence controller was employed to identify the fault type and perform a comparison of conditions to locate the faulty switch.

For the model-based method, the model was used to predict the outputs and compare them with the measured values to check and determine whether faults are occurring in the system [16,19,20]. In Reference [21], a Disturbance-Observer-Based model was used to estimate external disturbances and the unmodel dynamics and provide them to the torque reference. This system proves to be particularly effective in instances of torque fluctuations attributable to open-circuit conditions. Under such circumstances, the disturbance observer is responsible for determining the parameters necessary for the fault-tolerant switching table. This table plays a pivotal role in regulating the torque and stator flux, thereby improving the interference rejection ability of the system under open-circuit fault conditions. In Reference [22], a hybrid diagnosis method was proposed; there, a Luenburger observer was used to obtain the current residuals for estimating the three-phase currents. Then, the principle current analysis (PCA) and the support vector machine (SVM) were used to evaluate the current residuals to locate the faults. PCA was used to reduce the computational load on the classifier and refine the dataset into more distinct sample types, while SVM was applied to categorize and identify the specific type of fault. In [23], an adaptive sliding mode observers (SMOs) diagnosis method for detecting open-circuit faults in inverters used in PMSM drives was introduced. The comprehensive inverter system was decomposed into augmented and non-singular coordination transformations. SMOs were utilized to estimate the system state vector and calculate the residual error, enabling the determination of the fault's phase location and the identification of the faulty switch. In [24], an approach was introduced for diagnosing open-circuit faults in drives equipped with Model Predictive Current Control (MPCC). By utilizing MPCC, their model is capable of predicting currents and generating a corresponding cost function which the fault detection system uses for calculating a fault index. The subsequent stage involves a fault localization function that employs the calculated fault index to categorize the fault type based on predefined thresholds.

The data analysis method uses models based on data to analyze the conditions of the system and differentiate between normal states and various types of fault conditions. Several open-circuit fault diagnosis systems (OCFDS) based on machine learning methods have been developed for fault detection. In [25], modular multi-level converters (MMCs) were analyzed, and specific conditions (such as the current and voltage passing through the phase) were categorized based on the type of faulty conditions. A neural network (ANN) was trained under normal operating conditions and three different types of faulty operating conditions. The fault diagnosis system successfully classified the three types of faults in single-submodule open-circuit faults. Next, a fault localization system was employed, leveraging the ANN's output to determine the exact location of the faulty switches or capacitors. In [26], an improved support vector machine (SVM) was utilized for open-circuit fault identification in the fault diagnosis system. This improved SVM utilized an Overlapped Wavelet Packet Transform (MODWPT), significantly enhancing the feature extraction process for fault identification. The SVM effectively classifies the faults, leading to an approximate 3% increase in accuracy compared to conventional SVM methods. This

classifier was applied to determine faults within the submodule. In [27], a model data hybrid-driven method was proposed. The artificial neural network was trained with two datasets: one comprising experimental or simulation data and the other containing data from the analytical model of the power converters. The model was designed to extract and analyze fault features present in both datasets, encompassing a classification scheme that recognizes seven distinct patterns, including normal operation. The diagnostic capability of the model allows for the precise identification of faulty switches by analyzing input diagnostic variables. In [28], a 1D convolutional neural network (CNN) was trained using three-pole voltages under three different frequencies. The model was used to extract information on how variations in the modulation index and fundamental frequency influence pole voltages. A softmax function was used as its output layer, effectively classifying different types of faults occurring in submodule switches.

In traditional open-circuit fault diagnosis systems, the primary objective is to predict the phases that have experienced faults. However, the characteristics of multiple-phase motors are complex, involving considerations of intricate parameters. The current models have drawbacks, notably the lack of robustness and an inability to precisely identify specific faulty switches. This paper contributes in two significant ways: First, it implements neural networks into the open-circuit fault diagnosis system to enhance the accuracy in locating the faulty switch(es). Secondly, it determines an optimized neural network architecture suitable for application in the proposed open circuit fault diagnosis system.

## 2. Proposed Open-Circuit Fault Diagnosis System

In this paper, the main focus is on the operation of a three-phase Permanent Magnet Synchronous Motor (PMSM) with a three-phase inverter. The three-phase inverter comprises a total of six switches responsible for controlling the three-phase PMSM [29]. The configuration of the three-phase inverter is visually represented in Figure 1. In this circuit, three switches are positioned on the high side, while the remaining three are situated on the low side. Each pair of high-side and low-side switches forms a bridge that controls one phase of the motor [30]. It is important to note that the high-side and low-side switches must operate in complementary operation, meaning that only one switch in each pair can be closed at a time. For instance, if the high-side switch in a pair is closed, the low-side switch in that pair must be open, and vice versa.

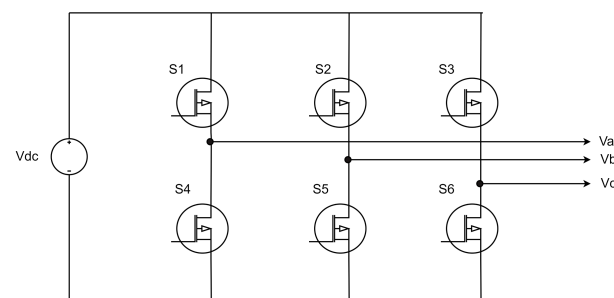


**Figure 1.** Structure of the electrical three-phase inverter.

### 2.1. Behaviour of the Open-Circuit Fault Diagnosis System

Figure 2 illustrates the space vector and sectors of the three-phase inverter. The possibility of various combination of the on and off states of the high-side switch was determined using the space vector voltage [12]. Within the space vector voltage, eight possible combinations were identified. The space vector was divided into six sectors, each evenly distributed in  $60^\circ$ , with vectors ( $V_1$ – $V_6$ ) representing these sectors [31]. It should be noted that two zero vectors were present in the space vector [20,30,32]. The normal switching sequences of the three-phase inverter are shown in Table 1, where State 0 and 7 corresponded to the zero vectors, while States 1 to 6 represented the normal switching sequences of the three-phase inverter.

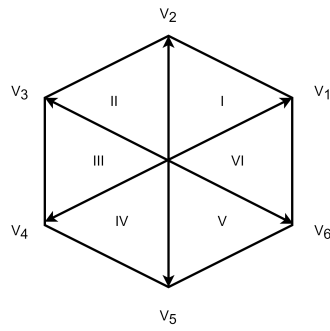


Figure 2. Space vector voltages of the three-phase inverter.

Table 1. Properties of normal-operation switching sequences.

State	Closed Switch	Line to Neutral Voltage			Phase to Phase Voltage		
		$V_U$	$V_V$	$V_W$	$V_{ab}$	$V_{bc}$	$V_{ca}$
0	-	0	0	0	0	0	0
1	S1, S5, S6	$2V_{DC}/3$	$-V_{DC}/3$	$-V_{DC}/3$	$V_{DC}$	0	$-V_{DC}$
2	S1, S2, S6	$V_{DC}/3$	$V_{DC}/3$	$-2V_{DC}/3$	0	$V_{DC}$	$-V_{DC}$
3	S2, S4, S6	$-V_{DC}/3$	$2V_{DC}/3$	$-V_{DC}/3$	$-V_{DC}$	$V_{DC}$	0
4	S2, S3, S4	$-2V_{DC}/3$	$V_{DC}/3$	$V_{DC}/3$	$-V_{DC}$	0	$V_{DC}$
5	S3, S4, S5	$-V_{DC}/3$	$-V_{DC}/3$	$2V_{DC}/3$	0	$-V_{DC}$	$V_{DC}$
6	S1, S3, S5	$V_{DC}/3$	$-2V_{DC}/3$	$V_{DC}/3$	$V_{DC}$	$-V_{DC}$	0
7	-	0	0	0	0	0	0

2.2. Type of Open-Circuit Fault

The proposed fault diagnosis aims to detect the specific damaged switch within the inverter. Figure 3 illustrates the structure of the switches in a phase with each of the phase comprising a high side and a low side. The proposed model is tailored to determine which switch has been damaged in that specific phase. There are two types of faults in one phase condition: (1) one switch fault, where either one of the switches is faulty and (2) two switch faults, where two of the switches are faulty. The states of each switch under normal conditions are clearly defined according to Table 1. Table 2 presents the response of the switches in one phase, along with the machine learning state labelling for all scenarios. For instance, when the machine learning state is one, it signifies that the high-side switch (Sa) has experienced a fault.

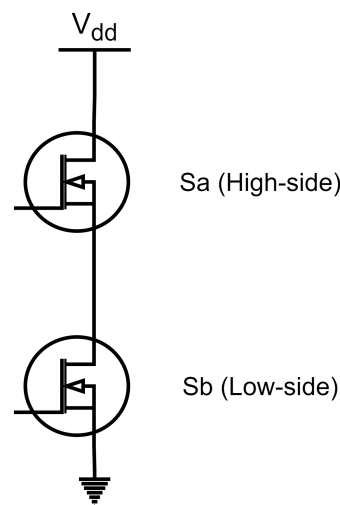


Figure 3. Structure of the switches in one phase.

**Table 2.** Properties of faulty operation switching sequences and machine learning state labelling.

Condition	Damaged Switch	Machine Learning State Labelling
Normal Condition	-	0
One switch fault	Sa Sb	1 2
Two switch fault	Sa and Sb	3

### 2.3. Type of Phase Fault

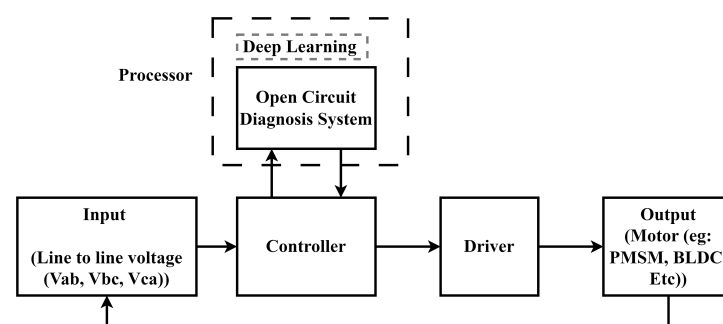
In the experiment, a three-phase permanent magnet synchronous motor (PMSM) was utilized. Three possible types of phase faults were considered: (1) one-phase fault—one of the phases in the motor system experiences a fault condition; (2) two-phases fault—any two of the phases in the motor system are faulty; (3) three-phases fault—all three phases are damaged and experience faults. Table 3 represents the machine learning labelling under normal phase conditions and faulty phase conditions.

**Table 3.** Normal and phase fault cases in machine learning labelling.

	Phase with Fault	Machine Learning State Label
Normal operation	None	0
One Phase Fault	U	1
	V	2
	W	3
Two Phases Fault	U, V	4
	U, W	5
	V, W	6
Three Phases Faults	U, V, W	7

## 3. Methodology of Developing Proposed Open-Circuit Fault Diagnosis System (OCFDS)

The proposed OCFDS comprised five main components: input (voltage (Line–Line)), controller, processor, three-phase inverter, and PMSM. The block diagram illustrating the structure of the open-circuit fault diagnosis system is shown in Figure 4.

**Figure 4.** Block diagram of proposed OCFDS.

### 3.1. Setup Arrangement and Flow of the Proposed Open-Circuit Fault Diagnosis System

The experiment utilized a PMSM motor, and its specifications are outlined in Table 4. In the neural network, signal standardization and filtering were essential steps before passing through the neural network. This standardization and filtering of the input were necessary to ensure that the signals were observable for the neural network to extract the fault features.

The experimental setup was depicted in Figure 5. Phase-phase voltage readings ( $V_{ab}$ ,  $V_{bc}$ ,  $V_{ca}$ ) were collected using an Arduino board functioning as the controller. These readings were then transmitted to the processor for the neural network to generate machine learning state labels, indicating the damaged switch. After receiving the output from the neural network, a signal was generated by the controller and transmitted to a Programmable Logic Controller (PLC). The PLC utilized this signal to control the Variable Frequency Drive (VFD), enabling the regulation of the motor's speed. Lastly, the phase-phase voltage readings were fed back to the controller for further analysis.

**Table 4.** PMSM motor information.

Description (Unit)	Value
Input AC Voltage (V)	220/230
Frequency (Hz)	100
Rated Torque (Nm)	12.8
Rated Speed (rpm)	3000
Rated Current (A)	8.6
Rated Power (kW)	4
No. of Poles	4

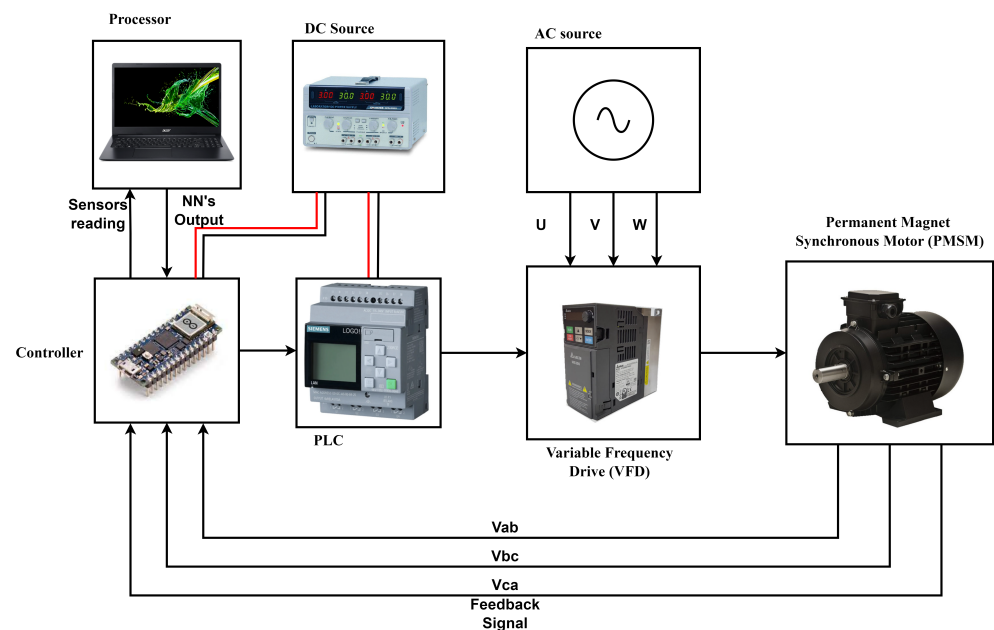


**Figure 5.** Experimental Setup of OCFDS.

Figure 6 illustrates a flow diagram of the open-circuit fault diagnosis system (OCFDS). The process begins with loading the neural network models (H5 files) and initializing variables. Subsequently, the system continuously monitors the phase-to-phase voltages, logging the data into a CSV file. These data undergo processing including filtering and standardization to facilitate feature extraction. The refined data are fed into the neural network models for each of the three phases to detect any faults. If a fault is detected, the corresponding phase neural networks generate output, which is transmitted to the classification system to identify the fault type and pinpoint the location of the faulty switch. Finally, the program returns to the initial state, perpetually monitoring the system.

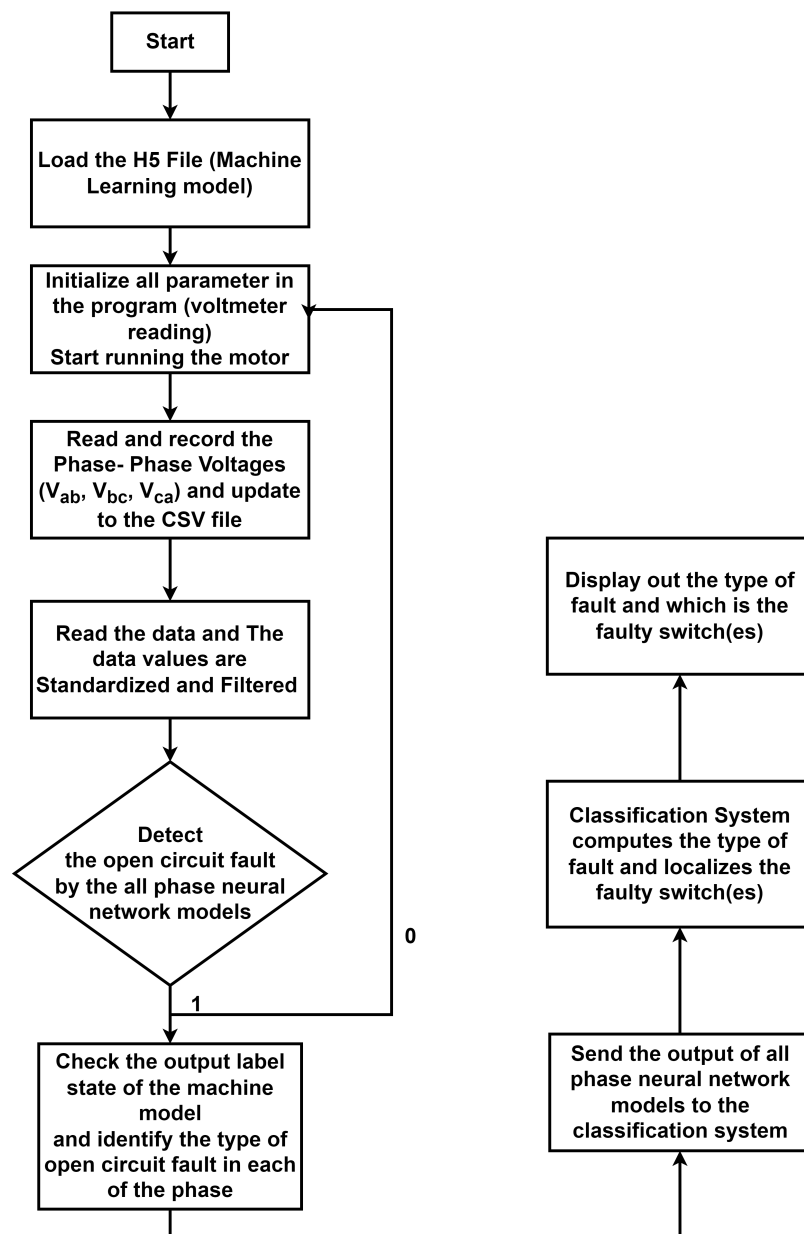


**Figure 6.** Flow diagram of OCFDS program.

### 3.2. Arrangement of the Neural Network

For the three-phase PMSM experiment, three distinct neural networks were developed to inspect each phase. Figure 7 illustrates the architecture of the proposed open-circuit fault diagnosis system's neural network, comprising two main components: (1) phase neural network and (2) classification system. Initially, the phase neural network comprises three specific neural networks dedicated to checking the phase and identifying the switch conditions within that specific phase. Subsequently, the classification system takes the output from all phase neural networks as input and utilizes it to identify faulty phases and locate switches experiencing faults. In the designed system, every phase neural network model is dedicated to a specific phase and utilizes phase-phase voltage data as input. This approach ensures that faults within individual phases are effectively detected. Once a fault is detected by the phase neural network, the classification system takes over. The classification system is responsible for identifying the type of fault and locating the faulty

switches, within the system. This setup ensures accurate fault detection and identification in the system.

The general structure of the neural network in the proposed open-circuit fault diagnosis system (OCFDS), as depicted in Figure 8, was implemented using the TensorFlow and Keras library in Python. Data are important in training the model, as they allow the neural network to effectively extract relevant features. For this purpose, phase-to-phase voltage data corresponding to various conditions are prepared and labeled according to the type of open-circuit fault present in each phase. Consequently, each neural network is trained on these labeled datasets to accurately identify and classify the type of open-circuit fault in its respective phase. The neural network models were designed to detect phase conditions and determine the status of all switches. The supervised learning method was employed to train all neural networks in the proposed open-circuit fault diagnosis system. Initially, input data undergoes signal processing for filtering and standardization, and the processed data is then fed through the neural network. Finally, the output layer generates outcomes, depending on the type of result. For instance, in the case of a multi-class classification model, the softmax activation function was deployed as the activation function for the output layer [33].

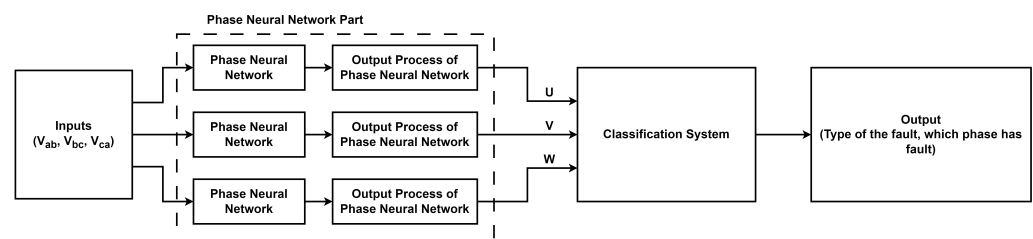


**Figure 7.** General structure of neural network used in the proposed open-circuit fault diagnosis system.

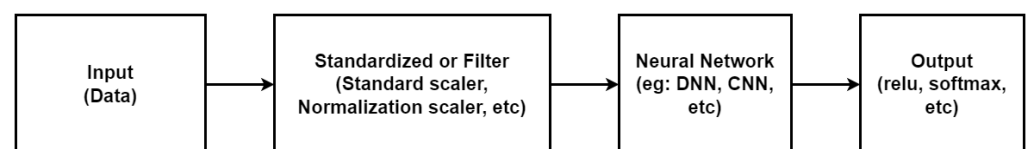


**Figure 8.** Structure of the open-circuit fault diagnosis system (OCFDS)'s neural network.

#### 4. Result and Discussion

In this paper, the proposed OCFDS consists of a three-phase neural network (U, V, W). All of these neural networks were developed using Python code with the Keras and TensorFlow libraries.

##### 4.1. Performance of Different Neural Network Architectures in Phase Neural Networks of Open-Circuit Fault Diagnosis System

The performance analysis of the open-circuit fault diagnosis system, considering various neural network architectures, is presented in Table 5. The experimental setup involved the examination of five distinct neural network types. Given the three phases in the motor (U, V, W), three separate phase neural networks were implemented. The comprehensive performance metrics are detailed in Table 6. Notably, only two neural network structures, namely Convolutional Neural Network (CNN) and Convolutional Neural Network-Long Short-Term Memory (CNN-LSTM), were successfully applied to the phase neural network. The LSTM (Long Short-Term Memory Neural Network) structure, on the other hand, proved to be unsuitable for implementation in this context due to its inability to capture the features of the open-circuit fault signal, resulting in lower and inconsistent accuracy. While the Deep Neural Network (DNN) and Artificial Neural Network (ANN) demonstrated feasibility in Phase U, their application in Phase V and Phase W failed to precisely determine faults, resulting in a notably low accuracy of approximately

30%. This limitation arose from the incapacity of DNN and ANN structures to effectively process the complex and inconsistent data inherent in the three-phase neural network. In contrast, CNN-LSTM and the 1D Convolutional Neural Network (CNN1D) exhibited comparable accuracy, achieving approximately 99.80% across all three phases in the neural networks. Both CNN1D and CNN-LSTM structures proved effective for implementation in this application, offering promising results in fault detection.

**Table 5.** Architecture of different types of neural networks models.

Layer	ANN	DNN	CNN1D
1	Dense (50, ReLu)	Dense (50, ReLu)	Conv1D (6, 3 ReLu)
2	Flatten	Flatten	MaxPooling1D (2, ReLu)
3	Dense (4, softmax)	Dense (24, ReLu)	Flatten
4	-	Dense (12, ReLu)	Dense (16, ReLu)
5	-	Dense (4, ReLu)	Dense (4, softmax)
6	-	Dense (4, softmax)	-
Training Duration	-	-	-

Layer	LSTM	CNNLSTM
1	LSTM (50, tanh)	Conv1D (6, 3 ReLu)
2	Dense (50, ReLu)	MaxPooling1D (2, ReLu)
3	Dense (25, ReLu)	Dense (50, ReLu)
4	Dense (12, ReLu)	LSTM (50, tanh)
5	Dense (4, ReLu)	Flatten
6	Dense (4, softmax)	Dense (4, softmax)

**Table 6.** Performance of the neural networks in all phases (UVW).

Neural Networks	Detection Accuracies (%)		
	Phase U	Phase V	Phase W
ANN	97.94	28.78	28.78
CNN	99.84	99.78	99.80
CNN-LSTM	99.87	99.80	99.80
DNN	99.74	28.79	28.78
LSTM	-	-	-

Figure 9 displays the confusion matrices for the CNN across all phases (U, V, W), demonstrating its capability to distinctly classify all labels with an accuracy of approximately 99% in identifying all conditions. Similarly, Figure 10 presents the confusion matrices for the CNN-LSTM across the same phases, achieving comparable results to the CNN with an accuracy of around 99% in identifying all conditions. The analysis of the confusion matrices for both CNN-LSTM and CNN1D highlights their exceptional proficiency in accurately identifying diverse states. Nonetheless, instances of misclassification were observed, primarily due to scenarios where signal overlap caused delays in accurately identifying the correct fault. Figure 11 shows the confusion matrices for the DNN across all phases (U, V, W), with a particular focus on the DNN's performance within the Phase U neural network. It is observed that, while the model excels in Phase U, accurately distinguishing between the four distinct labels in Phases V and W poses significant challenges. The graphical depiction reveals a relatively uniform spread of misclassifications across incorrect labels, indicating difficulties in achieving precise label discrimination. For example, in the classification of label 0, the model accurately predicted approximately 7000 instances, yet misclassified around 4000 instances into alternative labels, highlighting areas for improvement in model accuracy.

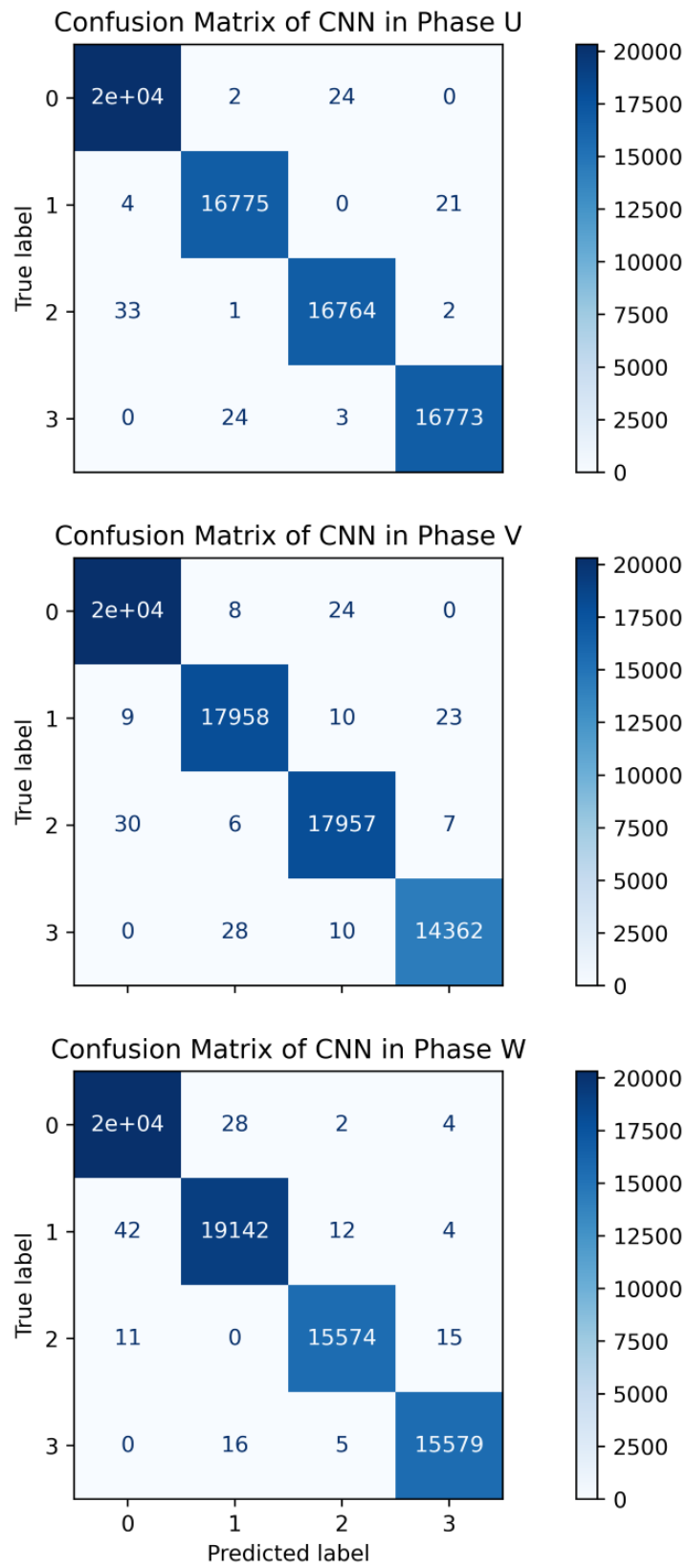


Figure 9. Confusion matrix for the performance of CNN1D.

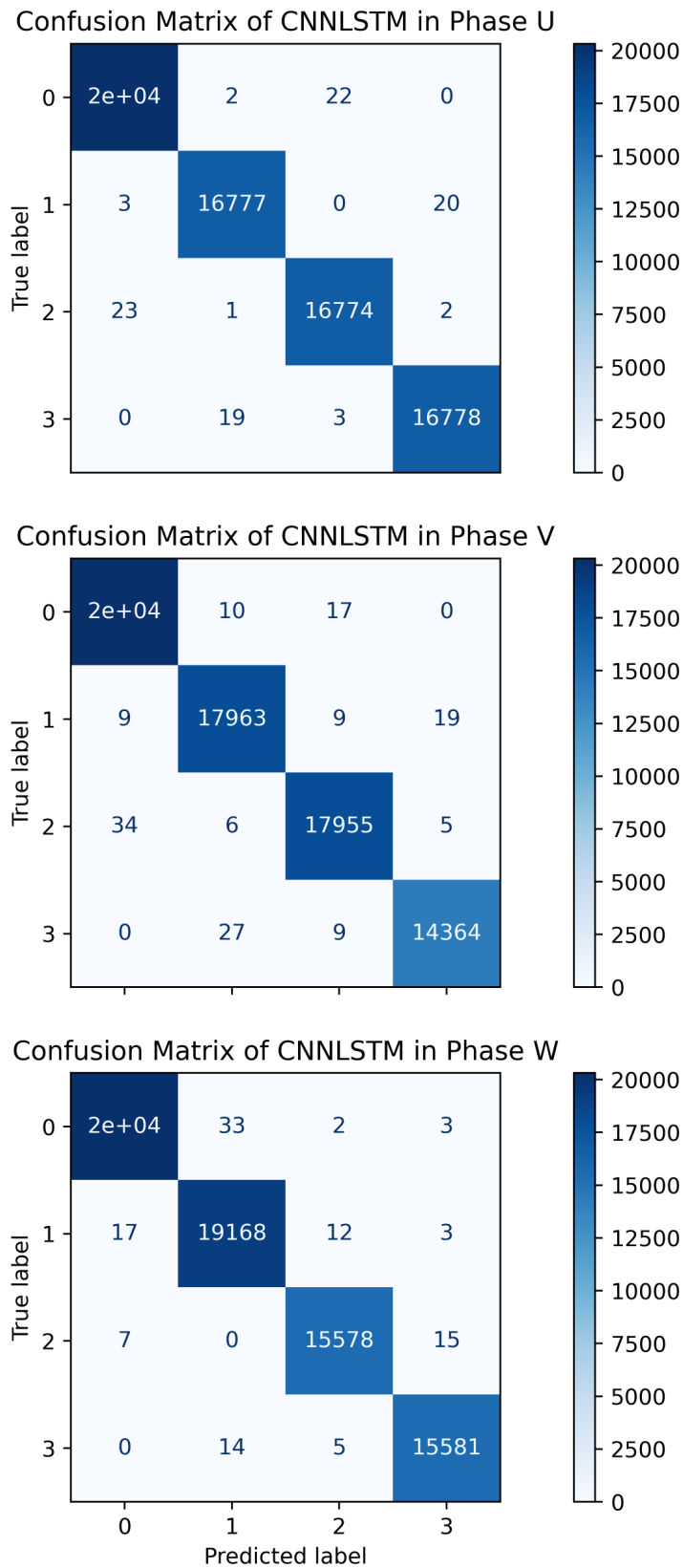
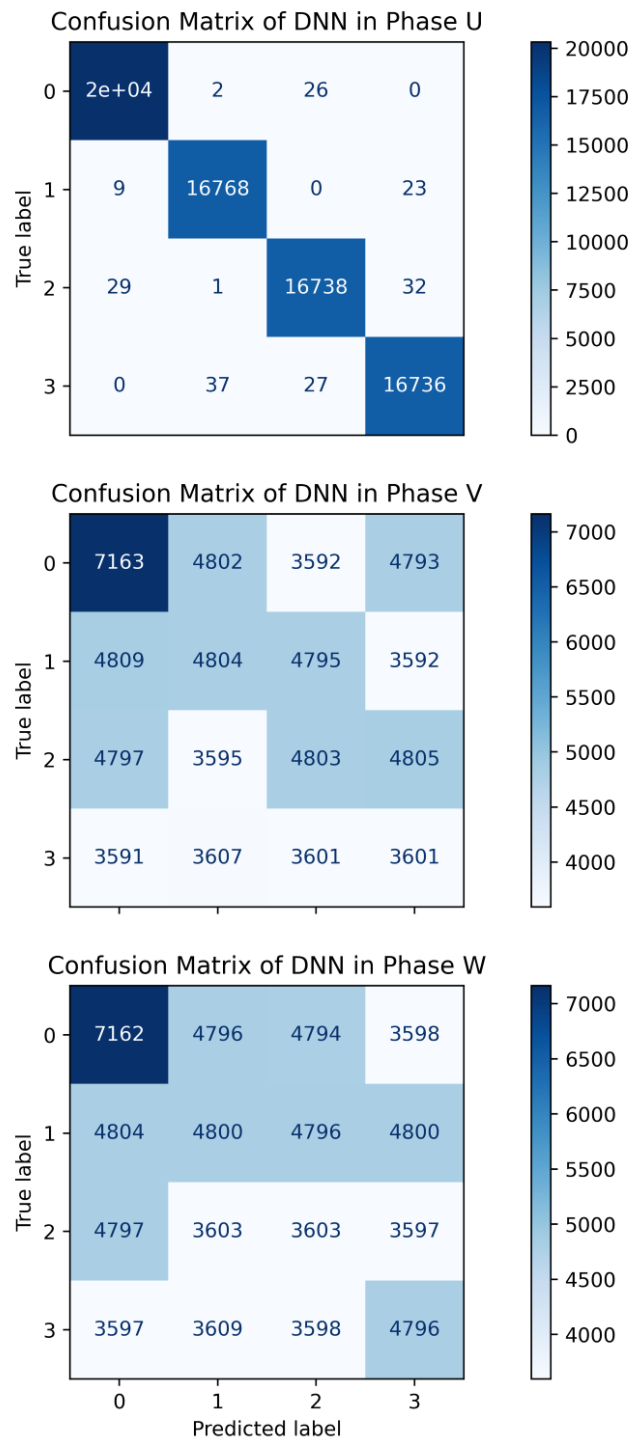


Figure 10. Confusion matrix for the performance of CNN-LSTM.



**Figure 11.** Confusion matrix for the performance of DNN.

All neural networks in OCFDS were trained using the Adam optimizer with a learning rate of 0.001 and a batch size of 20. Table 7 represents the performance accuracy of both CNN and CNN-LSTM models, differentiated by their respective numbers of hidden layers. The data in Table 7 reveal that the CNN-LSTM 2 configuration obtained the highest average accuracy. Among the CNN variants, the CNN 5 model had the highest average accuracy. Except for the CNN 4, CNN-LSTM 1, and CNN-LSTM 3 models, which fell slightly below, all other configurations consistently achieved an accuracy of approximately 99%.

**Table 7.** Comparison of the accuracy of CNN and CNN-LSTM model with different hidden layers in open-circuit fault diagnosis system.

	CNN 1	CNN 2	CNN 3	CNN 4	CNN 5
	Conv1D	Conv1D	Conv1D	Conv1D	Conv1D
	MaxPooling	MaxPooling	MaxPooling	MaxPooling	MaxPooling
	1D	1D	1D	1D	1D
	Flatten	Flatten	Flatten	Flatten	Flatten
	Dense	Dense	Dense	Dense	Dense
	-	Dense	Dense	Dense	Dense
	-	-	Dense	Dense	Dense
	-	-	-	Dense	Dense
	-	-	-	-	Dense
U Accuracy(%)	99.84	99.84	99.84	93.61	99.85
V Accuracy(%)	99.71	99.72	99.78	99.73	99.75
W Accuracy(%)	97.58	98.11	99.80	99.85	99.86
Average Accuracy(%)	99.04	99.22	99.81	97.73	99.82
	CNN-LSTM 1	CNN-LSTM 2	CNN-LSTM 3	CNN-LSTM 4	CNN-LSTM 5
	Conv1D	Conv1D	Conv1D	Conv1D	Conv1D
	MaxPooling	MaxPooling	MaxPooling	MaxPooling	MaxPooling
	1D	1D	1D	1D	1D
	LSTM	Dense	Dense	Dense	Dense
	Flatten	LSTM	Dense	Dense	Dense
	Dense	Flatten	LSTM	Dense	Dense
	-	Dense	Flatten	LSTM	Dense
	-	-	Dense	Flatten	LSTM
	-	-	-	Dense	Flatten
	-	-	-	-	Dense
U Accuracy(%)	99.84	99.84	95.02	99.81	99.85
V Accuracy(%)	87.61	99.80	99.77	99.84	99.77
W Accuracy(%)	99.80	99.84	94.73	99.82	99.82
Average Accuracy(%)	95.75	99.83	96.51	99.82	99.81

#### 4.2. Response of the Proposed Open-Circuit Fault Diagnosis System

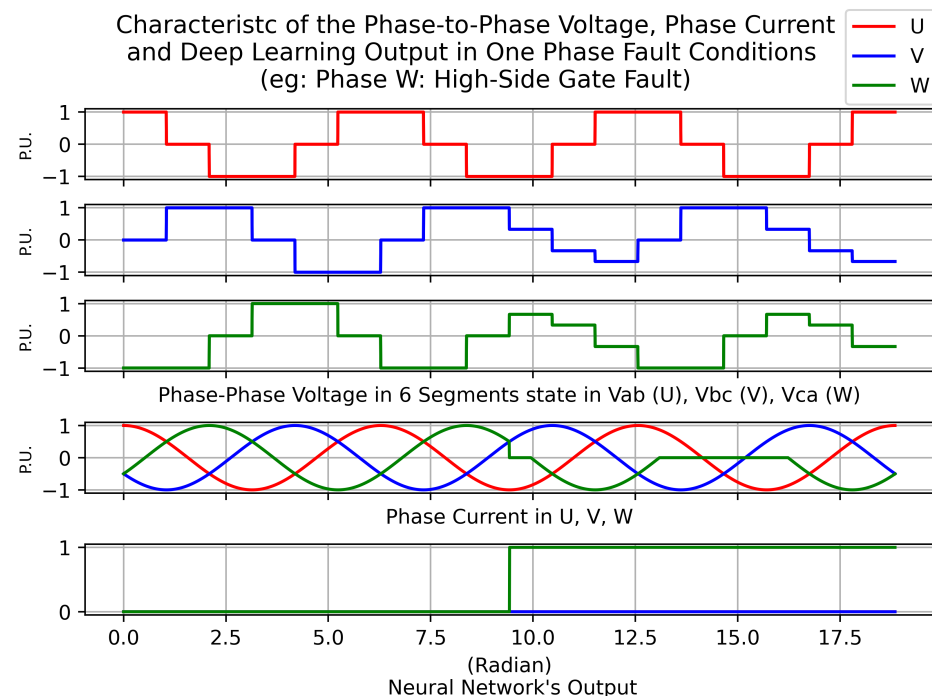
In this study, open-circuit faults within three-phase power systems were investigated using both simulation and experimental techniques to closely replicate real-world scenarios. In the simulation phase, open-circuit faults were digitally induced by the deliberate opening of switches within the circuit model, utilizing software tools such as Python or Matlab. This allowed for the analysis of the theoretical response of the system to faults in a controlled setting. In the experimental phase, open-circuit conditions were manually established in the experiment by disconnecting specific switches that are anticipated to fail under normal operational conditions. The simulation of open-circuit conditions was facilitated by a custom code that interrupted signal transmission to the switches, effectively creating an open-circuit scenario in the inverter.

Figure 12 illustrates the behavior of phase-to-phase voltage, phase current, and the performance of the three-phase neural network during an event where the high-side gate of Phase W was compromised due to a one-phase fault. This figure demonstrated that the fault became evident after three complete cycles of the Permanent Magnet Synchronous Motor (PMSM), specifically after a single cycle ( $2\pi$ ). Notably, the neural network dedicated to Phase W identified the fault at approximately  $8/3\pi$ , aligning with the moment the fault signal exclusively appeared. Observations revealed a significant decrease in the phase-to-phase voltages  $V_{bc}$  and  $V_{ca}$  at  $8/3\pi$ , along with an impact on the phase current in Phase W, where the positive current values became zero. This anomaly was attributed to the malfunction in the high-side gate of Phase W, which remained in an open-circuit condition.

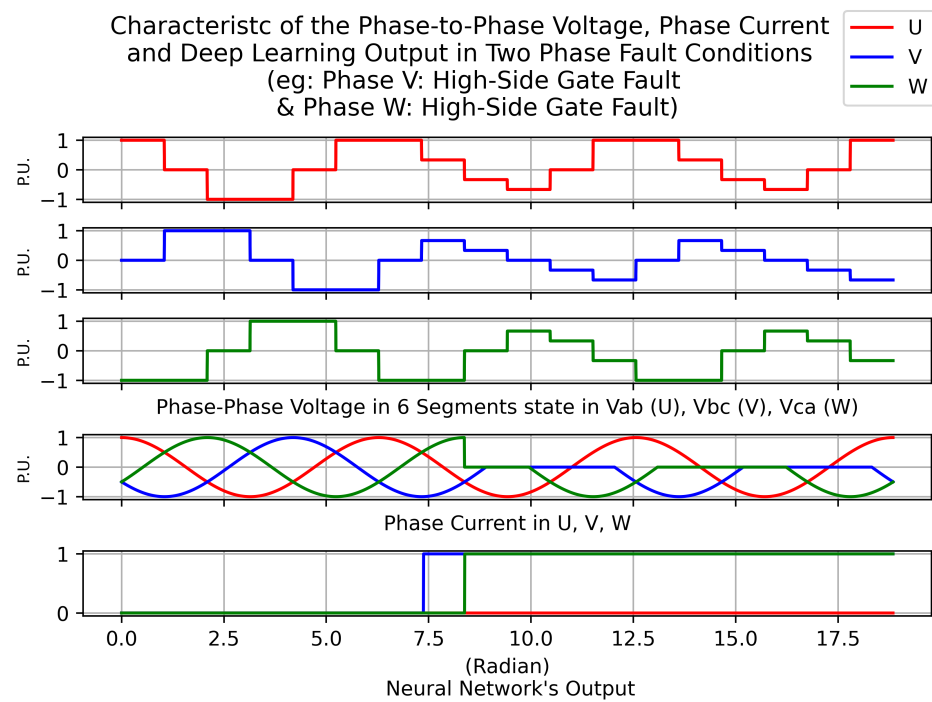
Consequently, the output from the Phase W neural network was set to one, indicating a fault in the high-side gate.

Figure 13 depicts the dynamics of phase-to-phase voltage, phase current, and the responses of the three-phase neural network during a scenario involving a two-phase fault, specifically affecting the high-side gates of Phase V and Phase W. In this situation, faults are identified in both phases. The phase-to-phase voltage  $V_{ab}$  experiences an increase of 0.3 per unit, while  $V_{bc}$  saw a decrease on the positive side by approximately 0.3 per unit and an increase on the negative side by about 0.3 per unit. Similarly,  $V_{ca}$  witnesses a decrease of 0.3 per unit on the positive side. Consequently, the positive phase currents in Phases V and W drop to zero, indicating that the high-side gates in both phases were compromised, leading to an open-circuit condition. The neural network for Phase V identifies the faults at  $7/3\pi$ , whereas the Phase W neural network detects the faults slightly later, at  $8/3\pi$ , due to the fault characteristics emerging at that specific moment. The outputs from the Phase V and Phase W neural networks are set to one, signifying the detection of high-side gate faults in the respective phases.

Figure 14 illustrates the characteristics of phase-to-phase voltage, phase current, and the responses of the three-phase neural network during a three-phase fault condition, which involved damage to the low-side gates of Phase U and Phase V, as well as the high-side gates of Phase V and Phase W. In this scenario, the negative side of the phase-to-phase voltage  $V_{ab}$  dropped to zero. For  $V_{bc}$ , there was a decrease on the positive side and an increase on the negative side. Similarly, the positive side of  $V_{ca}$  fell to zero. The phase current's positive side in Phases V and W dropped to zero, and the negative side of the phase current in Phase U also fell to zero, indicating a complete interruption. The Phase U Neural Network's output was two, indicating a fault in the low-side gate, whereas the outputs for the Phase V and W Neural Networks were one, signifying that the faults had occurred in the high-side gates. Notably, all three phase neural networks pinpoint the fault at  $2\pi$ .



**Figure 12.** Characteristics of the phase-to-phase voltage, phase current, and deep learning output in one-phase fault conditions (eg: Phase W: high-side gate fault).



**Figure 13.** Characteristics of the phase-to-phase voltage, phase current, and deep learning output in two-phase fault conditions (eg: Phase V: high-side gate fault and Phase W: high-side gate fault).

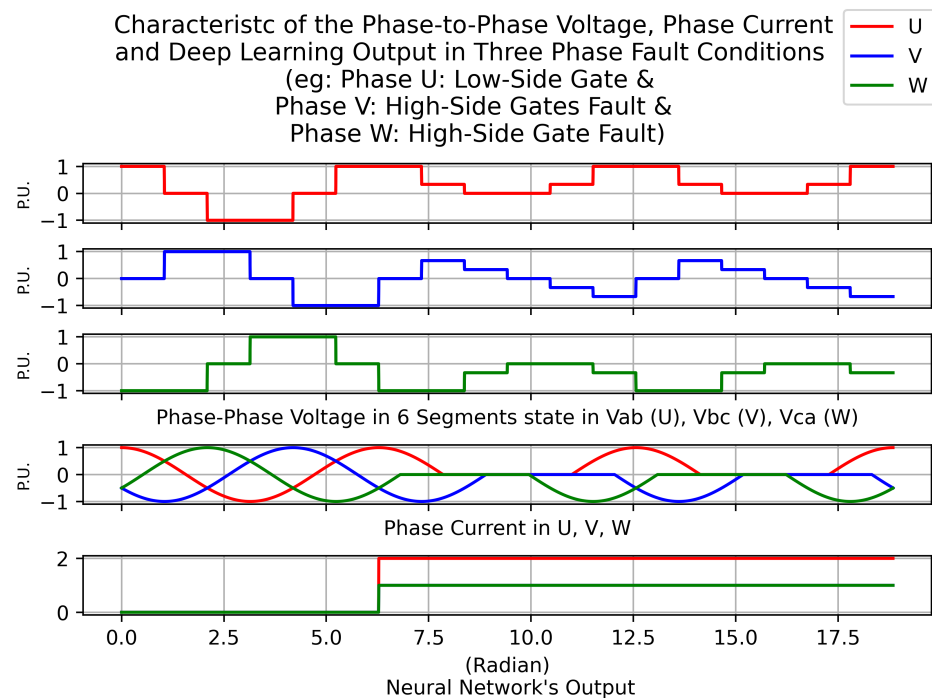


**Figure 14.** Characteristics of the phase-to-phase voltage, phase current, and deep learning output in three-phase fault conditions (eg: Phase U: low-side gate fault and Phase V: low and high-side gate fault and Phase W: high-side gate fault).

### 5. Conclusions

In this study, two neural networks models, namely the CNN and CNN-LSTM models, were successfully implemented in the proposed open-circuit fault diagnosis system. Both models demonstrated high accuracy in detecting various faults across all three phases. Notably, both architectures achieved a similar detection performance. The experimental

results confirm that the proposed system can achieve an overall detection accuracy of approximately 99.8%. In the first scenario, where a one-phase fault affected the high-side gate of Phase W, the fault was precisely detected after three oscillations of the Permanent Magnet Synchronous Motor (PMSM) at  $2\pi$ . In the second scenario, involving a two-phase fault affecting both Phase W and Phase V, the neural networks identified the faults at  $8/3\pi$  for Phase W and  $7/3\pi$  for Phase V. The delayed response of the Phase W neural network was attributed to fault signals closely resembling normal signals, resulting in a more gradual identification. In the third scenario, a three-phase fault impacting the low-side gates of Phase U and Phase V, along with the high-side gates of Phase V and Phase W, was concurrently pinpointed by all three-phase neural networks at  $2\pi$ . Overall this system effectively identifies the specific phase where the fault occurs, enabling the localization of faulty switches within the inverter.

**Author Contributions:** Conceptualization, K.S.K.C.; methodology, K.S.K.C.; software, K.S.K.C.; validation, K.S.K.C.; formal analysis, K.S.K.C., K.W.C.; investigation, K.S.K.C.; resources, K.W.C.; data curation, K.S.K.C.; writing—original draft preparation, K.S.K.C.; writing—review and editing, K.S.K.C., K.W.C., Y.C.C. and S.M.; visualization, K.W.C., Y.C.C. and S.M.; supervision, K.W.C. and Y.C.C.; project administration, K.W.C. and Y.C.C.; funding acquisition, K.W.C., Y.C.C. and S.M. All authors have read and agreed to the published version of the manuscript.

**Funding:** This research was funded by Universiti Tunku Abdul Rahma Research Fund (UTARRF) Project No IPSR/RMC/UTARRF/2023-C2/C03.

**Data Availability Statement:** Data are contained within the article.

**Conflicts of Interest:** The authors declare no conflict of interest.

## References

1. Fan, Y.; Cui, R.; Zhang, A. Torque Ripple Minimization for Inter-Turn Short-Circuit Fault Based on Open-Winding Five Phase FTFSCW-IPM Motor for Electric Vehicle Application. *IEEE Trans. Veh. Technol.* **2020**, *69*, 282–292. [\[CrossRef\]](#)
2. Cao, C.; Wang, Z.; Duan, C.; Wang, X. Fault-Tolerant Control of Dual Three-Phase PMSM Drives with Inter-Turn Short-Circuit Fault. In Proceedings of the 2021 IEEE 13th International Symposium on Diagnostics for Electrical Machines, Power Electronics and Drives (SDEMPED), Dallas, TX, USA, 22–25 August 2021. [\[CrossRef\]](#)
3. Kumar, P.H.; Lakhimsetty, S.; Somasekhar, V.T. An Open-End Winding BLDC Motor Drive With Fault Diagnosis and Autoreconfiguration. *IEEE J. Emerg. Sel. Top. Power Electron.* **2020**, *8*, 3723–3735. [\[CrossRef\]](#)
4. Choi, U.M.; Lee, J.S.; Blaabjerg, F.; Lee, K.B. Open-Circuit Fault Diagnosis and Fault-Tolerant Control for a Grid-Connected NPC Inverter. *IEEE Trans. Power Electron.* **2015**, *31*, 7234–7247. [\[CrossRef\]](#)
5. Salehifar, M.; Arashloo, R.S.; Moreno-Equilaz, J.M.; Sala, V.; Romeral, L. Fault Detection and Fault Tolerant Operation of a Five Phase PM Motor Drive Using Adaptive Model Identification Approach. *IEEE J. Emerg. Sel. Top. Power Electron.* **2014**, *2*, 212–223. [\[CrossRef\]](#)
6. Guefack, F.L.T.; Kiselev, A.; Kuznietsov, A. Improved Detection of Inter-turn Short Circuit Faults in PMSM Drives using Principal Component Analysis. In Proceedings of the 2018 International Symposium on Power Electronics, Electrical Drives, Automation and Motion (SPEEDAM), Amalfi, Italy, 20–22 June 2018. [\[CrossRef\]](#)
7. Orłowska-Kowalska, T.; Wolkiewicz, M.; Pietrzak, P.; Skowron, M.; Ewert, P.; Tarchala, G.; Krzysztofiak, M.; Kowalski, C.T. Fault Diagnosis and Fault-Tolerant Control of PMSM Drives—State of the Art and Future Challenges. *IEEE Access* **2022**, *10*, 59979–60024. [\[CrossRef\]](#)
8. Wang, X.; Wang, Z.; Xu, Z.; Cheng, M.; Wang, W.; Hu, Y. Comprehensive Diagnosis and Tolerance Strategies for Electrical Faults and Sensor Faults in Dual Three-Phase PMSM Drives. *IEEE Trans. Power Electron.* **2019**, *34*, 6669–6684. [\[CrossRef\]](#)
9. Ullah, Z.; Hur, J. Analysis of Inter-Turn-Short Fault in an FSCW IPM Type Brushless Motor Considering Effect of Control Drive. *IEEE Trans. Ind. Appl.* **2020**, *56*, 1356–1367. [\[CrossRef\]](#)
10. Halder, S.; Bhat, S.; Bhaumik, C.; Rakshit, R. Stator Inter-Turn Fault Diagnosis in Permanent Magnet Synchronous Motor. In Proceedings of the 2020 IEEE First International Conference on Smart Technologies for Power, Energy and Control (STPEC), Nagpur, India, 25–26 September 2020. [\[CrossRef\]](#)
11. Wang, X.; Wang, Z.; Gu, M.; Xiao, D.; He, J.; Emadi, A. Diagnosis-Free Self-Healing Scheme for Open-Circuit Faults in Dual Three-Phase PMSM Drives. *IEEE Trans. Power Electron.* **2020**, *35*, 12053–12071. [\[CrossRef\]](#)
12. Gou, B.; Ge, X.; Wang, S.; Feng, X.; Kuo, J.B.; Habetler, T.G. An Open-Switch Fault Diagnosis Method for Single-Phase PWM Rectifier Using a Model-Based Approach in High-Speed Railway Electrical Traction Drive System. *IEEE Trans. Power Electron.* **2016**, *31*, 3816–3826. [\[CrossRef\]](#)

13. Sun, J.; Li, C.; Zheng, Z.; Wang, K.; Li, Y. A Generalized, Fast and Robust Open-Circuit Fault Diagnosis Technique for Star-connected Symmetrical Multiphase Drives. *IEEE Trans. Energy Convers.* **2022**, *37*, 1921–1933. [[CrossRef](#)]
14. Chen, T.; Pan, Y. A Novel Diagnostic Method for Multiple Open-Circuit Faults of Voltage-Source Inverters Based on Output Line Voltage Residuals Analysis. *IEEE Trans. Circuits Syst. II Express Briefs* **2021**, *68*, 1343–1347. [[CrossRef](#)]
15. Chen, Y.; Liang, S.; Li, W.; Liang, H.; Wang, C. Faults and Diagnosis Methods of Permanent Magnet Synchronous Motors: A Review. *Appl. Sci.* **2019**, *9*, 2116. [[CrossRef](#)]
16. Jiang, C.; Liu, H.; Wheeler, P.; Wu, F.; Cai, Z.; Huo, J. A Novel Open-Circuit Fault Detection and Location for Open-End Winding PMSM Based on Differential-Mode Components. *IEEE Trans. Ind. Electron.* **2022**, *69*, 7776–7786. [[CrossRef](#)]
17. Gonzalez-Prieto, I.; Duran, M.J.; Rios-Garcia, N.; Barrero, F.; Martin, C. Open-Switch Fault Detection in Five-Phase Induction Motor Drives Using Model Predictive Control. *IEEE Trans. Ind. Electron.* **2018**, *65*, 3045–3055. [[CrossRef](#)]
18. Lee, H.W.; Lee, K.B. Open-Circuit Fault Diagnosis and Fault-Tolerant Operation of Dual Inverter for Open-End Winding Interior Permanent Magnet Synchronous Motor. In Proceedings of the 2022 IEEE 5th Student Conference on Electric Machines and Systems (SCEMS), Busan, Republic of Korea, 24–26 November 2022. [[CrossRef](#)]
19. Xu, J.; Guo, S.; Guo, H.; Tian, X. A Novel Diagnostic Method for Single and Dual Power Switch Open-Circuit Faults of Six-Phase FTPMSM System Even in Fault Tolerant Operation. *IEEE Trans. Power Electron.* **2022**, *37*, 9777–9789. [[CrossRef](#)]
20. Trabelsi, M.; Semail, E.; Nguyen, N.K.; Meinguet, F. Open-switch and open-phase real time FDI process for multiphase PM Synchronous Motors. In Proceedings of the 2016 IEEE 25th International Symposium on Industrial Electronics (ISIE), Santa Clara, CA, USA, 8–10 June 2016. [[CrossRef](#)]
21. Zhou, H.; Xu, J.; Chen, C.; Tian, X.; Liu, G. Disturbance-Observer-Based Direct Torque Control of Five-Phase Permanent Magnet Motor Under Open-Circuit and Short-Circuit Faults. *IEEE Trans. Ind. Electron.* **2021**, *68*, 11907–11917. [[CrossRef](#)]
22. Zhang, Z.; Luo, G.; Zhang, Z.; Tao, X. A hybrid diagnosis method for inverter open-circuit faults in PMSM drives. *CES Trans. Electr. Mach. Syst.* **2020**, *4*, 180–189. [[CrossRef](#)]
23. Xu, S.; Chen, X.; Liu, F.; Wang, H.; Chai, Y.; Zheng, W.X.; Chen, H. A Novel Adaptive SMO-Based Simultaneous Diagnosis Method for IGBT Open-Circuit Faults and Current Sensor Incipient Faults of Inverters in PMSM Drives for Electric Vehicles. *IEEE Trans. Instrum. Meas.* **2023**, *72*, 1–15. [[CrossRef](#)]
24. Huang, W.; Du, J.; Hua, W.; Lu, W.; Bi, K.; Zhu, Y.; Fan, Q. Current-Based Open-Circuit Fault Diagnosis for PMSM Drives with Model Predictive Control. *IEEE Trans. Power Electron.* **2021**, *36*, 10695–10704. [[CrossRef](#)]
25. Ke, Z.; Pan, J.; Na, R.; Potty, K.; Zhang, J.; Wang, J.; Xu, L. Single-Submodule Open-Circuit Fault Diagnosis for a Modular Multi-level Converter Using Artificial Intelligent-based Techniques. In Proceedings of the 2019 IEEE Applied Power Electronics Conference and Exposition (APEC), Anaheim, CA, USA, 17–21 March 2019. [[CrossRef](#)]
26. Geng, Z.; Wang, Q.; Han, Y. IGBT Open Circuit Fault Diagnosis Based on Improved Support Vector Machine. In Proceedings of the 2021 8th International Conference on Information, Cybernetics, and Computational Social Systems (ICCSS), Beijing, China, 10–12 December 2021. [[CrossRef](#)]
27. Li, Z.; Gao, Y.; Zhang, X.; Wang, B.; Ma, H. A Model-Data-Hybrid-Driven Diagnosis Method for Open-Switch Faults in Power Converters. *IEEE Trans. Power Electron.* **2021**, *36*, 4965–4970. [[CrossRef](#)]
28. Apsari, D.P.; Jung, J.; Lee, D.C. Open-Circuit Fault Diagnosis Based on Deep Learning for Four-Level Active Neutral-Point Clamped Inverters. In Proceedings of the 2023 11th International Conference on Power Electronics and ECCE Asia (ICPE 2023-ECCE Asia), Jeju Island, Republic of Korea, 22–25 May 2023. [[CrossRef](#)]
29. Agustin, C.A.; Yu, J.t.; Lin, C.K.; Fu, X.Y. A Modulated Model Predictive Current Controller for Interior Permanent-Magnet Synchronous Motors. *Energies* **2019**, *12*, 2885. [[CrossRef](#)]
30. Huang, W.; Du, J.; Hua, W.; Fan, Q. An open-circuit fault diagnosis method for PMSM drives using symmetrical and DC components. *Chin. J. Electr. Eng.* **2021**, *7*, 124–135. [[CrossRef](#)]
31. Li, X.; Li, S.; Chen, W.; Shi, T.; Xia, C. A Fast Diagnosis Strategy for Inverter Open-Circuit Faults Based on the Current Path of Brushless DC Motors. *IEEE Trans. Power Electron.* **2023**, *38*, 9311–9316. [[CrossRef](#)]
32. Lemma, B.D.; Pradabane, S. Control of PMSM Drive Using Lookup Table Based Compensated Duty Ratio Optimized Direct Torque Control (DTC). *IEEE Access* **2023**, *11*, 19863–19875. [[CrossRef](#)]
33. Chollet, F. *Deep Learning with Python, Second Edition*; Manning Publications Co. LLC: New York, NY, USA, 2021; p. 400.

**Disclaimer/Publisher's Note:** The statements, opinions and data contained in all publications are solely those of the individual author(s) and contributor(s) and not of MDPI and/or the editor(s). MDPI and/or the editor(s) disclaim responsibility for any injury to people or property resulting from any ideas, methods, instructions or products referred to in the content.